

High-performance cellulose based nanocomposite soft actuators with porous high-conductivity electrode doped by graphene-coated carbon nanosheet

Zhuangzhi Sun · Shanqi Du · Fei Li · Lu Yang · Dan Zhang · Wenlong Song

Received: 4 April 2018 / Accepted: 16 August 2018 / Published online: 20 August 2018
© Springer Nature B.V. 2018

Abstract A nanocomposite soft actuator based on porous high-conductivity electrode membrane, which was composed of biopolymer cellulose mixed with chitosan and highly conductive nanoparticles generated by reduced graphene oxide encapsulated multi-walled carbon nanotube, was developed in this paper. No new substance was discovered in the regenerated electrode layer through the scanning analysis from FT-IR and XRD. Actuators exhibited significant enhancement in peak to peak displacement, which was 3.64 times increased than the traditional value at 5 V 0.1 Hz. With the test of solid-state electric double layer capacitor, actuators showed the highest specific capacitance (10.695 F g^{-1}) at the current density of 1 A g^{-1} , the lowest internal resistance ($9.2 \text{ } \Omega \text{ g}^{-1}$) in

the frequency range of 10^5 – 10^{-2} Hz, and the lowest energy density (901 Wh kg^{-1}) at the current density of 10 A g^{-1} , which demonstrated the absolute advantages in the conductivity and channels for electrons. These findings suggest that research on porous high-conductivity electrode layer holds great promise in the further study of higher performance actuators.

Keywords Cellulose · Soft actuator · Nanoparticles · Porous · Conductivity · Electrode

Introduction

Recently, Electroactive Polymers (EAPs) have received great attention due to their attractive characteristics of biomimetic actuation, large deformation, quick response, flexibility and light weight, etc. (Acome et al. 2018; Acerce et al. 2017a, b; Kotal et al. 2016a, b). Thus, EAPs have been considered as a challenging nature-inspired technology for various applications such as soft electronics (Wang et al. 2016; Jang et al. 2017), biomimetic robots (Kim et al. 2015; Yuk et al. 2017; Altinkaya et al. 2016), bio-medical devices (Lasprilla et al. 2012), and biomimetic sensor-actuators (Barrios 2018; Terasawa and Asaka 2018; Ozdemir et al. 2015). Among the various EAPs actuators, ionic polymer gel-based actuators, which are composed of electrolyte layer sandwiched by two high conductivity electrodes, have emerged as

Z. Sun (✉) · S. Du · F. Li · L. Yang · W. Song (✉)
Province Key Laboratory of Forestry Intelligent
Equipment Engineering, School of Mechanical and
Electrical Engineering, Northeast Forestry University,
Harbin 150000, People's Republic of China
e-mail: sunzhuangzhi@nefu.edu.cn

W. Song
e-mail: wlsong@nefu.edu.cn

Z. Sun · W. Song
Ministry of Education Key Laboratory of Bio-based
Material Science & Technology, Northeast Forestry
University, Harbin 150000, People's Republic of China

D. Zhang
College of International Education, Harbin Institute of
Technology, Harbin 150000, People's Republic of China

promising candidates due to their large actuation deformation and air working stability under low voltage. This kind of actuators can store electrical energy in a double interface and convert it into mechanical properties by reversible ion intercalation and deintercalation of electrodes. Therefore, electrodes, including low-dimensional carbon materials with large specific surface areas and high electrical conductivity, play a very important role in presenting high-performance electrochemical-mechanical behavior of ionic polymer gel-based actuator (Terasawa and Asaka 2017; Fang et al. 2017; Wang et al. 2017a, b; Acerce et al. 2017a, b).

At present, many studies have been carried out on the improvement of conductivity and the formation of stable ion channels in the electrode layer on the performance improvement of ionic actuators. Many achievements have been gained. Muralidharan et al. (2016) prepared chitosan/reduced graphene oxide (RGO) nanocomposite optical actuators by a simple solvent casting method, and the actuation behavior could be tuned either by tuning the RGO content or by tuning the applied pre-strain. Lu et al. (2012a, b, 2013) researched a highly stable air working bimorph actuator, and graphene-stabilized silver nanoparticle electrochemical electrode and graphene nanosheet/carbon nanotube hybrid electrode could significantly improve electromechanical properties. Sun et al. (2017a, b) provided a naturally crosslinked chitosan based ionic actuator with cathode deflection phenomenon, and multi-wall carbon nanotubes (MCNT) and MnO_2 composite electrode were investigated. Recent studies have found that the formation of pore structures in electrode layer contributed to promote the electromechanical properties, Chen et al. (2017) illustrated that the high actuation performance of actuators was rooted in the hierarchical pore structure with dominant size < 2 nm, the optimal pyridinic nitrogen active sites (6.78%) and the effective conductivity (382 S m^{-1}) of the electrodes. Therefore, the porous structure formed inside the electrode layer contributed to the improvement of electromechanical performance of actuators.

Thus, the above research results show that scholars were focused on studying various ways to enhance specific surface areas and electrical conductivity characteristics of the electrode layer by doping reduced graphene oxide (RGO) or multi-wall carbon nanotube (MCNT). Scholars have admitted that the

enhancement of the specific capacitance and the conductivity of the electrode layer by the doping of RGO and MCNT could further improve the electromechanical performance of actuators. However, the regularity of the ratio of the conductive particles (MCNT and RGO) was lacked, and the optimal ratio of conductive particles (MCNT and RGO) has not been confirmed. Moreover, the method of promotion by the porous structure formed inside the electrode layer, which contributed to the electromechanical performance of actuators, was worth being explored. Therefore, the effects of the forming porous structure inside the electrode layer to achieve the optimal doping ratio of the conductive particles on enhancing the electromechanical performance of ionic actuators were worth being studied.

Hence, based on the porous structure of polymer cellulose (Wu et al. 2015; Wang et al. 2017a, b; Xin et al. 2017), in this paper, a porous high-conductivity electrode layer, which was supported by chitosan-mixed cellulose porous framework structure and doped by graphene-coated carbon nanosheet was prepared. Based on this porous highly conductive electrode layers, a high-performance cellulose regenerated actuator was fabricated, and under different mass fractions of MCNT and RGO inside nanocomposite electrode membrane, the electromechanical and electrochemical characteristics of ionic actuators were analyzed.

Material and method

Cellulose (α -Cellulose content of 87%) was purchased from Aladdin Chemistry Co., Ltd. (Shanghai, China.) with the polymerization degree of 1484 and the molecular weight of 240 kDa. Ionic liquid (IL) involving 1-Butyl-3-methylimidazolium chloride ([Bmim]Cl, molecular weight 174.67 and melting point 70°C) was obtained from Lanzhou Institute of Physical Chemistry, Chinese Academy of Sciences (Lanzhou, China) and used as received. High purity natural multi-walled carbon nanotubes (MCNT, deionized water solvent, 70 wt% carbon nanotube content) was purchased from Boyu Gaoke New Materials Technology Co., Ltd., Beijing, China. Some commonly used chemical reagents (lithium chloride (LiCl), glycerol, etc.) were purchased from Yongchang Reagents Co., Ltd., Harbin, China.

Preparation of Re-Cel based actuators

10 mL of experimental [Bmim]Cl was added into the beaker evenly. And it was stirred under a temperature of 75 °C and heated for 20 min. Then, 1.0 g of cellulose was added to IL mixture weighed by an analytical balance, and the mixture was stirred at low speed uniformly with the stirring time for 40 min and the temperature for 75 °C. The prepared regenerated cellulose (Re-Cel) solution was sonicated and was defoamed for 30 min. At room temperature and humidity, the mixed solution was smeared on a glass plate of 100 mm × 100 mm. After that, it was then placed in distilled water for 30 min. The Re-Cel membrane was removed on the glass plate and was allowed to dry in the air for 2 h.

The polymer mixture solution was prepared in a chitosan and cellulose mass ratio of 1:2 under 2% acetic acid solution. Certain quality scores MCNT and RGO aqueous dispersion were added to the mixed solution to prepare a mixed solution of composited electrode membrane. A magnetic stirrer was applied to stir the mixed solution, which was stationary for 2 h. The newly prepared Re-Cel based electrolyte was coated with the composite electrode film solution on the upper and lower surface, and the composited membranes were placed to dry at room temperature. Re-Cel based actuator was obtained through Re-Cel electrolyte membrane and porous MCNT–RGO composite electrode membranes, which was cut into the size of 3.5 mm × 5 mm (as shown in Fig. 1).

Actuation mechanism of Re-Cel based actuators

The IL-Cel solution was smeared on a clean glass plate and placed in deionized water during the film formation of the electrolyte membrane. Due to the existence of a competitive hydrogen bond between water and cellulose hydroxyls, these bonds between Cl[−] and hydroxyl groups in cellulose were weakened or even interrupted, resulting in the majority solution of Cl[−] ions.

Under the action of electric excitation, the electric double layer was formed on both sides of electrode membrane as the charge injected. Some of the positively charged cations Bmim⁺ were immobilized by the hydrogen bonding of cellulose, and the dissociated anions Cl[−] moved toward the anode side of the electrode under Van der Waals force. As the

concentration gradually increased with time, the concentration of Cl[−] on the anode side of the electrode increased. When both sides of the concentration reached a certain value, a significant concentration difference appeared. The ions inside ionic actuator showed the cathode deflection appeared under the action of Van Der Waals force and anion volumetric strain, as shown in Fig. 1.

Experimental methods

In this experiment, the electrochemical properties of Re-Cel based actuator were mainly measured as follows. The characteristic peaks of the functional group of the samples were analyzed using a Nicolet iS50 Fourier Transform Infrared Spectrometer (FT-IR) with a spectral range of 4000–500 cm^{−1}. The Phase analysis of the material composition and structure was carried out on a PANalytical X'Pert3 Powder X-ray diffractometer (XRD) at a scanning range of 5–55° and a scanning speed of 5°/min. The cyclic voltammetry (CV), ect. were tested by using a multi-channel chemical test station (Corrtest CS350H) and the electrolyte solution was 1 mol/L^{−1} H₂SO₄. The morphology was characterized by a scanning electron microscope (SEM, JEOL JSM-6480). A tensile test was used an electromechanical universal testing machine (AG-A10T) with a tensile speed of 10 mm/min. All measurement data presented here were an average of three samples. The electromechanical properties of IL-Cel based actuator were experimented by our experimental platform (Sun et al. 2017b). The specific capacitance *C* of regenerated electrolyte membrane was calculated by the Eq. (1). Here, *v* was the voltage sweep rate. Δ*E* was the potential drop over the entire cycle, and *E*₁ and *E*₂ were the lowest and highest voltage during the cycle.

$$C = \frac{\int_{E_1}^{E_2} idE}{2v\Delta E} \quad (1)$$

Results and discussion

SEM analysis

Figure 2a–g were the cross-section of electrode layer with different mass fractions of MCNT and RGO.

Figure 2a–f can be found that several RGO sheet existed in the SEM cross-section of the electrode layer. This was due to a large number of MCNT coated on the three-dimensional RGO sheet, and made it impossible to see the distribution of RGO sheets in the electrode layer. Figure 2a was the cross-section of electrode layer with MCNT particles. It can be seen that MCNT was loosely arranged in the interior of the electrode membrane, and there were a large number of voids between them, which affected the flexibility and the conductivity of the electrode layer to some extent. However, the electrode membrane with MCNT and RGO formed a clad block structure by RGO effectively filled the gap between MCNT obtained the

Fig. 2 SEM cross-section of electrode layer with different MCNT–RGO: **a** 2.3–0%, **b** 2.3–0.04%, **c** 2.3–0.11%, **d** 2.3–0.2%, **e** 0–0.11%, **f** 1.3–0.11%, **g** 3.3–0.11%

improvement of electrical and mechanical properties. Figure 2e showed SEM section of the electrode layer including RGO sheet. It can be seen that RGO layer was evenly distributed inside the electrode layer, which presented the effects on the increase of the specific surface area inside the electrode and forming the frame support. Figure 2a–d showed that with increasing RGO content and unchanged MCNT content, the bulk structure of MCNT coated RGO

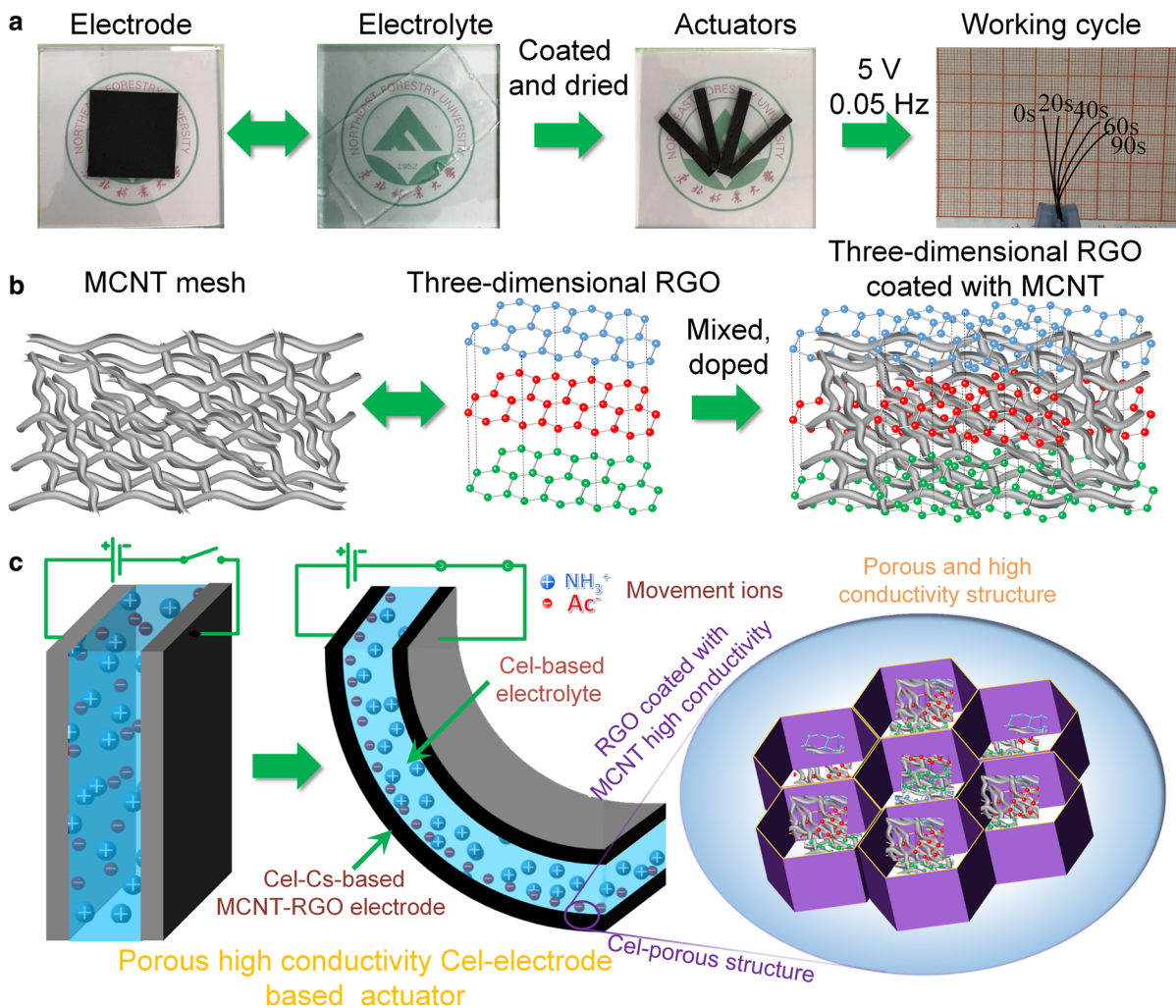
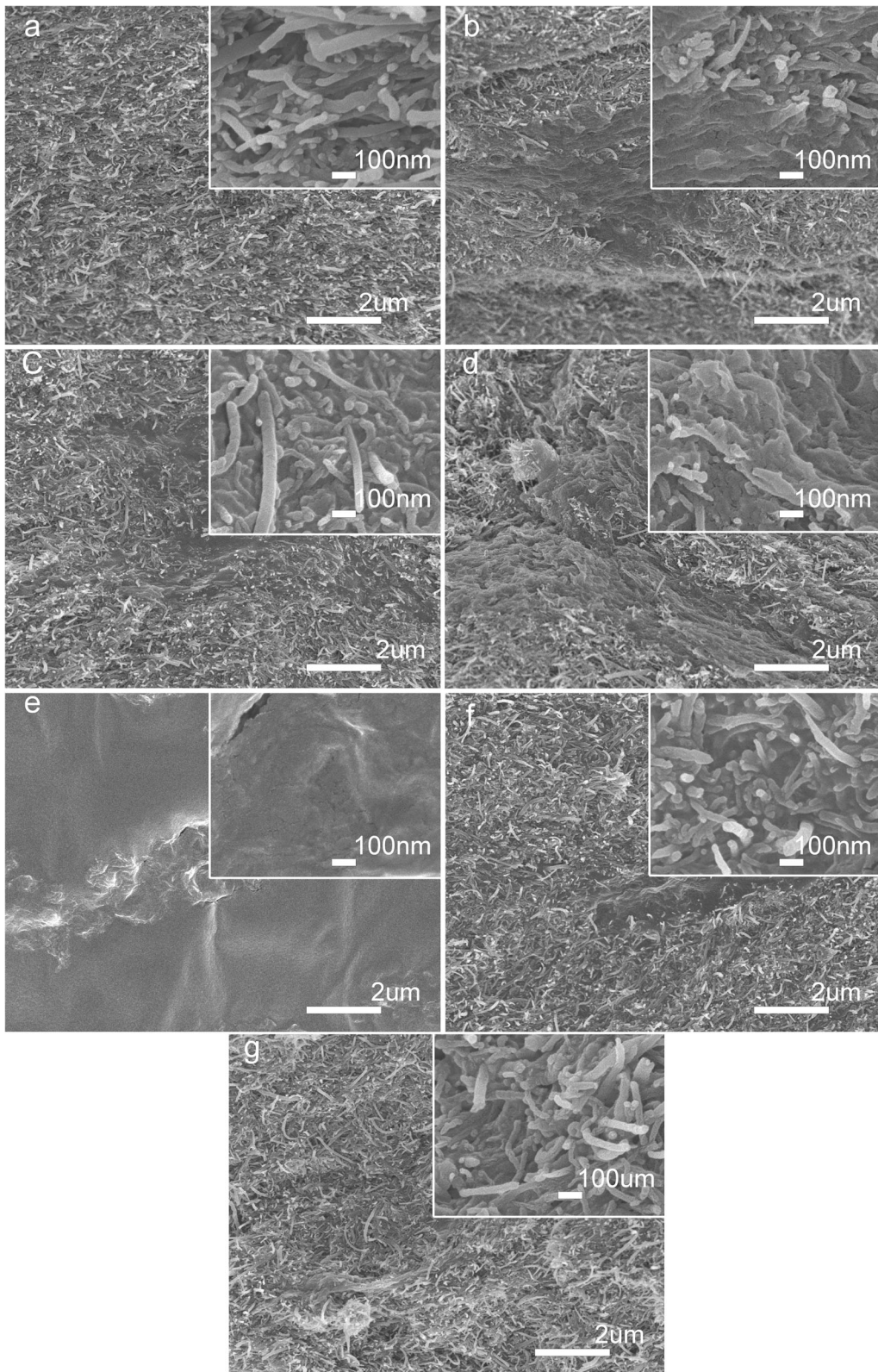


Fig. 1 Cellulose regenerated nanocomposite actuators: **a** experimental preparation and testing process **b** structure of highly conductive porous electrode layer **c** schematic diagram of actuator with highly conductive porous electrode layer



increased, which could effectively increase the specific surface area inside the electrode membrane.

FT-IR and XRD scanning

Figure 3a showed XRD curves of electrode layers under different MCNT and RGO content. It can be seen that the diffraction peaks of the pure chitosan film were at 13.3° , 18.1° , and 19.7° , and a new peak appeared in the doped electrode layer. The RGO-doped electrode layer showed a strong absorption peak at 21.59° . The trend of peaks of the electrode film doped with MCNT and MCNT–RGO in XRD was basically the same, and it showed new peaks at 26.5° , 43.1° , and 45.1° . These new diffraction peaks were due to the addition of functional groups of MCNT and RGO. Compared with XRD of MCNT–RGO-doped electrode layer and MCNT-doped electrode layer, the value of the diffraction peak slightly decreased due to the inhibitory effect of RGO. The XRD curves of the RGO-doped electrode layer and RGO–MCNT-doped electrode layer had completely different diffraction peaks. This was due to the structure of RGO-coated MCNT formed in the electrode layer, and the internal structure appeared a certain change. Also, MCNT wrapped around RGO. When the X-ray particles were emitted, they collided with MCNT and reflected back. Thus, most of the expressed functional groups were MCNT functional groups. Compared to XRD images of pure chitosan films, the diffraction peaks of chitosan itself after doping disappeared. The content of MCNT and RGO was relatively large, which completely

covered chitosan. So the functional group strength of RGO and MCNT was significantly greater than that of chitosan.

Figure 3b showed FT-IR curves of electrode layers with different content of MCNT and RGO. It can be seen that in pure chitosan, the stretching vibration peaks of $-\text{NH}$ and $-\text{OH}$ was at about 3268.5 cm^{-2} , and the stretching vibration peak of $-\text{CH}_2$ was at about 2876.5 cm^{-2} . The stretching vibration peaks of $\text{C}-\text{O}$ group were at 1659 cm^{-2} and 1031 cm^{-2} ; 1406 cm^{-2} and 1328.7 cm^{-2} were $-\text{CN}$ peak, and the $-\text{NH}$ and $-\text{OH}$ groups were assigned at 3253.9 cm^{-2} . Comparing electrode layers under different content of MCNT and RGO and pure chitosan layer, it could be seen that due to the inhibition of RGO, the absorption peaks of doped electrode layers were significantly reduced. New peaks appeared at 2359.9 cm^{-2} and 1998.4 cm^{-2} due to the addition of MCNT and RGO. The FT-IR images of MCNT-doped, RGO-doped, and MCNT–RGO-doped electrode layers were basically the same, and no new peaks generated or absorption peaks disappeared because the functional groups contained in MCNT and RGO were basically the same. However, MCNT-doped electrode layer had a slightly higher absorption peak due to the lack of RGO inhibition. FT-IR curves of the pure chitosan film compared with the remaining three groups of doped electrode layers showed that the absorption peaks of pure chitosan film disappeared, and after doping with MCNT and RGO, the peak of the absorption peak of the electrode was reduced. Because the functional groups contained in RGO and MCNT were

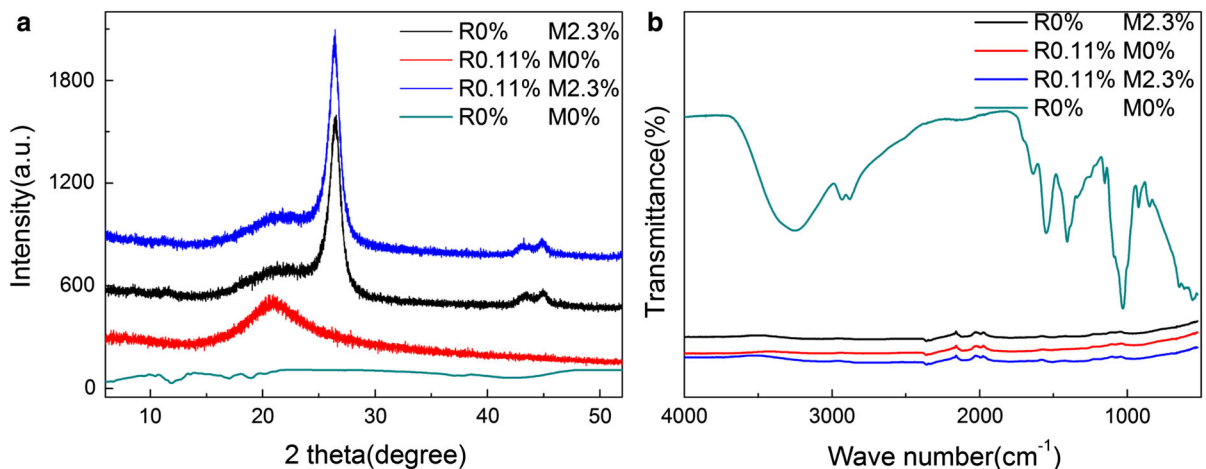


Fig. 3 XRD curves (a) and FT-IR curves (Carbohydrate) of electrode layers with various MCNT and RGO

significantly stronger than the functional groups contained in chitosan after doping with MCNT and RGO. Thus, the absorption peak of chitosan was masked in the figure. A three-dimensional block structure was formed by MCNT coated RGO. Since the functional groups of MCNT and RGO were basically the same, there was no chemical reaction inside the substance and structural change during the infrared spectroscopy experiment. The trend of the FT-IR curve was basically the same, and the diffraction peak had no positional deflection.

CV

Figure 4a–f were CV curves of electrode layer under different mass fraction MCNT–RGO at the scanning voltage range of $-0.4\text{ V} \sim 0.7\text{ V}$ and the scanning rate of 5 mV s^{-1} , 10 mV s^{-1} , 20 mV s^{-1} . It can be seen that when the MCNT content was constant, the redox peak of CV curve increased significantly with increase of the RGO content, and the electrical activity of the electrode layer became significantly stronger. However, with the increase of RGO content, the trend of peak curve changed slower, and when the content of RGO was 0.11%, the redox peak of the electrode layer was relatively lower. Thus, the content of RGO and MCNT was not as good as possible, but when there was a stable ratio, the electrode layer showed the best electrochemical capacitance characteristics, as shown in Table 1 and Fig. 4a, c, e. When the RGO content was constant, the peak value of the redox peak first increased and then decreased with the increase of MCNT content. The redox peaks at the mass fraction of 0.1% RGO and 1.3% MCNT were the largest, and the redox characteristics of the electrode layer were best, as shown in Table 2 and Fig. 4b, d, f. The capacitance values of the electrode layer were calculated by the area of the graph in CV curves. By comparing with the different rate samples in Fig. 4g, it can be seen that with the increase of the scanning rate, the specific capacitance all decreased. At the mass fraction of 0.1% RGO and 1.3% MCNT, the specific capacitance of the electrode layer was significantly greater than all other electrode layers, which indicated that the electrode layer had the largest capacitance at this content. Under this ratio of mass fraction MCNT–RGO (R 0.11% and M 1.3%), the electrode layer had excellent conductivity over other ratios, and the internal three-dimensional porous structure was more

reasonable. At the same time, in the assembled application of actuators, under the same voltage excitation, the charge and discharge speed of actuators based on this mass fraction of electrode layer was faster, and the effect of forming a stable electric field on both sides of actuator was better. Thus, the actuation performance of actuators generated significant improvement in the response speed of the actuators.

GCD

Figure 5 showed the GCD curves of electrode layers with different mass fractions MCNT–RGO at current densities of 1 A g^{-1} , 5 A g^{-1} , and 10 A g^{-1} . The experiment adopted a time-based charge and discharge test method, and the electrolyte was $1\text{ mol L}^{-1}\text{ H}_2\text{SO}_4$ solution. When the time was fixed, with the increase of the specific capacitance, the potential changed small. It can be seen that the specific capacitance of the electrode layer with 0.11% RGO⁻¹ and 3% MCNT was much higher than that of the other groups of electrode layers. When the current density increased, the MCNT-doped electrode layer and the RGO-doped electrode layer tended to increase in specific capacitance, which was suitable to work under high current conditions. Irrespective of RGO-doped and MCNT-doped electrode layers, specific capacitance of the remaining electrode layers tended to decrease first, and then increase. This indicated that when a large current was applied to the electrode layers, the active substance adsorbed a large amount of H^+ ions in a short time, so that ions concentration at the interface between the active substance and the electrolyte rapidly decreased. The ion diffusion rate in the electrolyte layer could not satisfy the number of ions required for charge and discharge of the electrode, resulting in the increase in polarization caused by liquid phase diffusion at the interface of electrode. Then, the charge response on the electrode lagged behind the voltage change, which caused loss of capacitance of the electrode during charge and discharge of large currents. When the current continued to increase, water molecule in the electrolyte was electrolyzed, and a large amount of H^+ ions were generated. So H^+ ions in the solution were replenished, and the specific capacitance of electrode layers rose again. At the same current density, the specific capacitance of the electrode layer prepared by

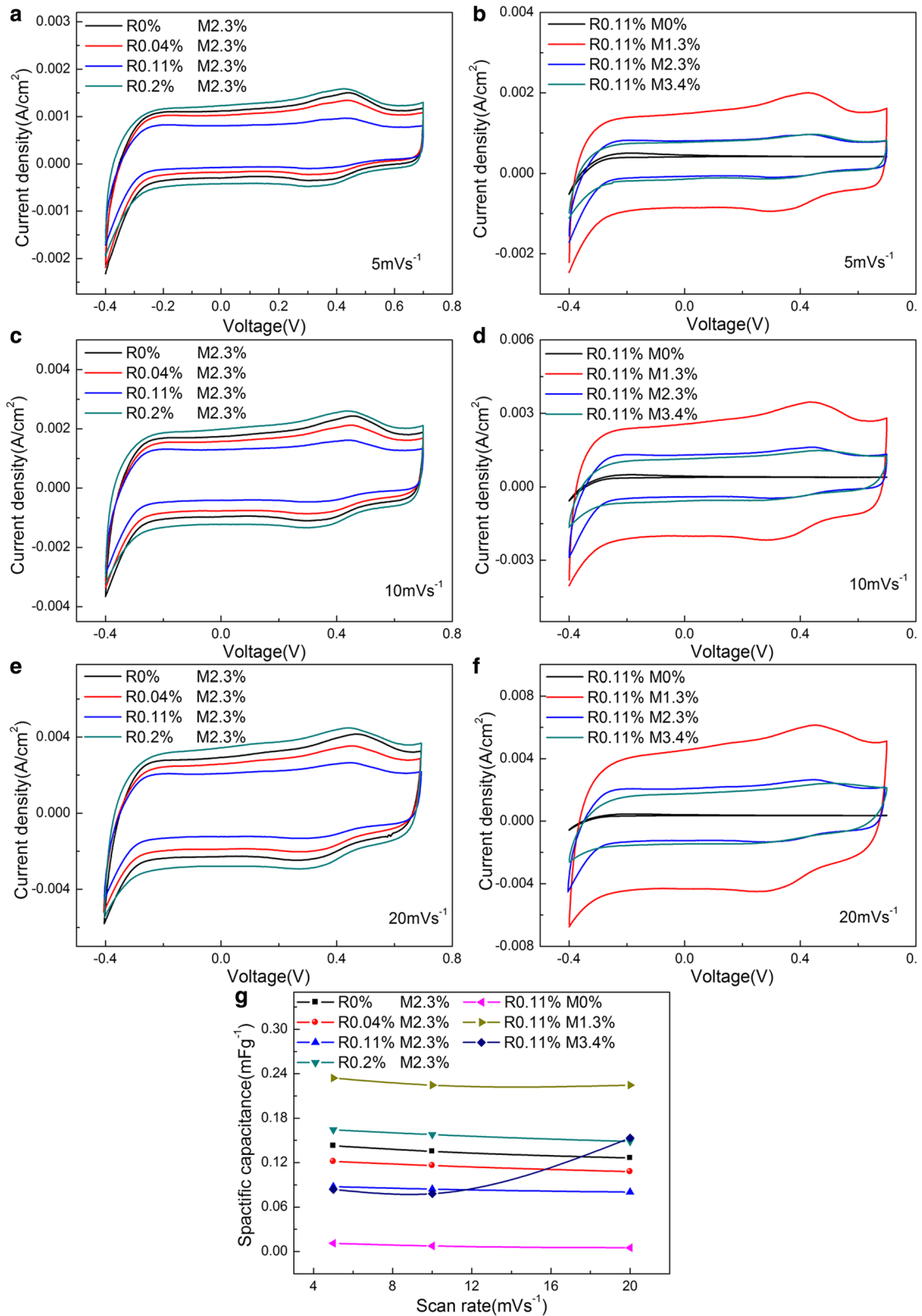


Fig. 4 CV curves of electrode layer under different mass fractions MCNT–RGO: **a** RGO mass fraction at 5 mVs^{-1} **b** MCNT mass fraction at 5 mVs^{-1} **c** RGO content of MCNT–RGO at different sweep speeds

0.11% RGO and 1.3% MCNT was much higher than that of the other groups. The electrode layers doped with RGO and MCNT caused the formation of a structure formed by MCNT coated on the surface of the RGO increased the specific surface area inside the electrode layer. However, excessive RGO or excessive MCNT content may cause uneven distribution of the structure, resulting in a decrease in the electrochemical properties. Therefore, by comparing the specific capacitances of different samples at the same current density, it can be seen that the structure formed by made of 0.1% RGO and 1.3% MCNT was evenly distributed in the electrode layer, and the electrode layer presented the optimal electrochemical properties. According to the calculated specific capacitance C , the energy density E can be further calculated by the formula of $E = 1/2C(\Delta V)^2$. Figure 5h showed the energy density curves at different current densities. It can be seen from the analysis that the energy density of doped electrode layers with different contents of MCNT–RGO was significantly better than that of electrode layers doped with RGO, and the energy density tended to be similar.

Table 1 Specific capacitance of different RGO-doped electrode layers at various sweep speeds

Speed (mv s^{-1})	Samples			
	2.3% MCNT 0% RGO (mF mm^{-2})	2.3% MCNT 0.04% RGO (mF mm^{-2})	2.3% MCNT 0.11% RGO (mF mm^{-2})	2.3% MCNT 0.2% RGO (mF mm^{-2})
5	0.14266	0.12166	0.087687	0.16442
10	0.13528	0.11605	0.084204	0.15778
20	0.12634	0.10794	0.080194	0.14861

Table 2 Specific capacitance of different MCNT-doped electrode layers at various sweep speeds

Speed (mv s^{-1})	Sample				
	0% MCNT 0.11% RGO (mF mm^{-2})	1.3% MCNT (mF mm^{-2})	0.11% RGO	2.3% MCNT 0.11% RGO (mF mm^{-2})	3.4% MCNT 0.11% RGO (mF mm^{-2})
5	0.011077	0.15322		0.087687	0.23422
10	0.0075536	0.078017		0.084204	0.22453
20	0.0052427	0.083738		0.080194	0.20978

EIS

Here, AC impedance spectrum of samples at 10^5 Hz to 0.01 Hz was measured by three-electrode electrochemical system with $1 \text{ mol L}^{-1} \text{ H}_2\text{SO}_4$ solution. Figure 6 was EIS curves of electrode layer prepared by different content of MCNT and RGO. It can be seen that the slope of the low frequency indicated the speed of ion diffusion. The ion diffusion rate of the electrode layer prepared by 0.1% RGO and 1.3% MCNT was much larger than that of other electrode layers. This showed that the internal structure of the electrode layer was uniform, and the void structure of the electrode layer was regular. At the same time, there were many free MCNT and RGO in the electrode layer which meant that not all MCNT and RGO could become mutually overlapping structures. When the mixed ratio of MCNT and RGO was different, the diffusion rate of ions would be affected. Thus, ion diffusion rates in the electrode layers did not all increase with the increase of the doping ratio. In the high frequency, the equivalent resistance of the mixed MCNT–RGO doped electrode layer was significantly smaller than that of the electrode layer doped with MCNT or RGO. This indicated that the composite structure formed by RGO and MCNT effectively increased the specific surface area of the electrode layer, and the internal void structure of the electrode, which significantly improved the conductive characteristics of the

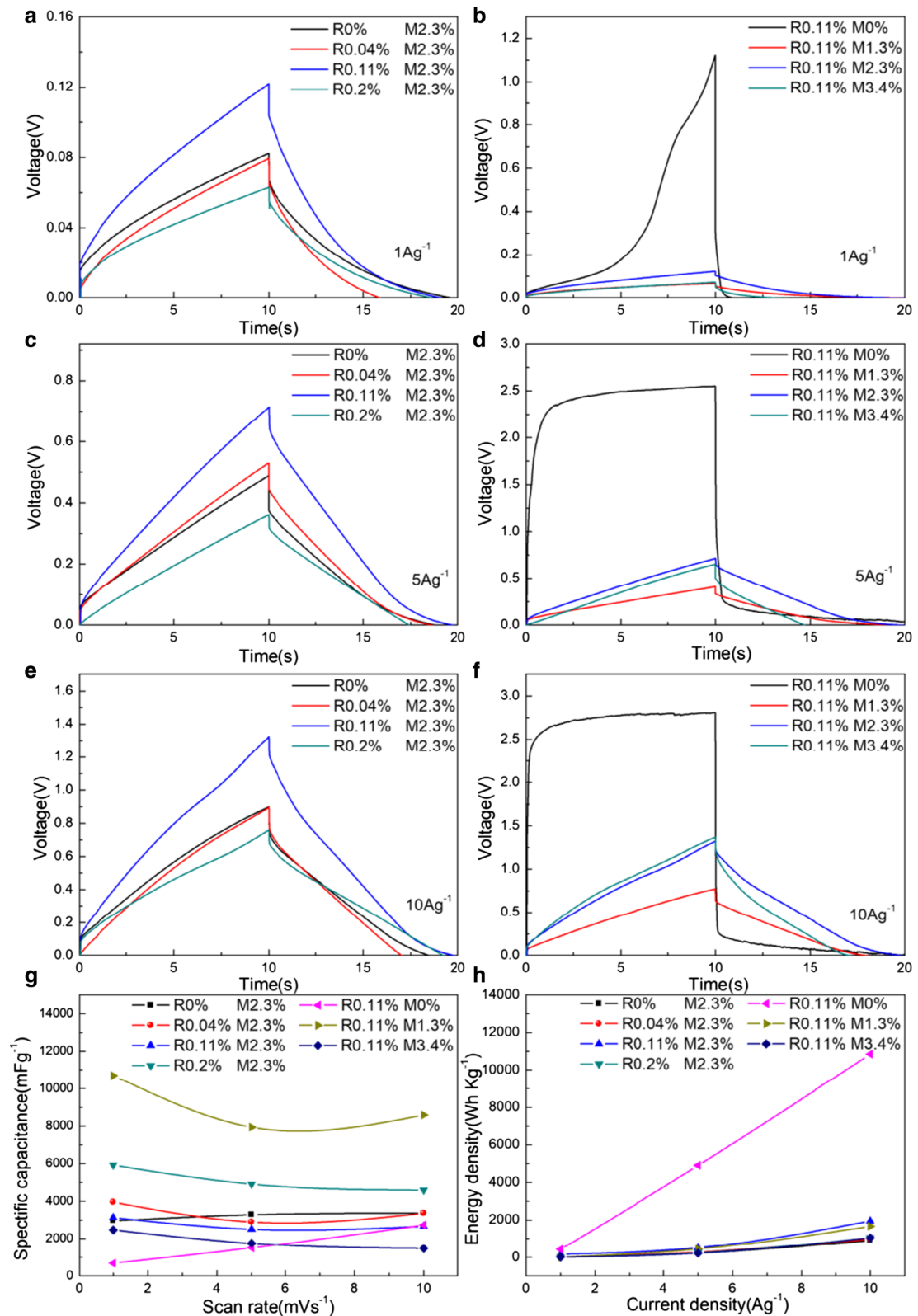


Fig. 5 GCD curves of electrode layers at different mass fractions MCNT–RGO: **a** RGO mass fraction at 1Ag^{-1} **b** MCNT mass fraction at 1Ag^{-1} **c** RGO mass fraction at 5Ag^{-1} **d** MCNT mass fraction at 5Ag^{-1} **e** RGO mass fraction at 10Ag^{-1} **f** MCNT mass fraction at 10Ag^{-1} **g** Specific capacitance at different MCNT–RGO mass fraction **h** Energy densities under different mass fractions MCNT–RGO at current densities of $1\text{Ag}^{-1} \sim 10\text{Ag}^{-1}$

electrode layer. The diameter of the arc formed by the high frequency was the charge transfer resistance R_{ct} . The electrode layers prepared with 0.1% RGO and 1.3% MCNT had the smallest resistance of $9.2\ \Omega\ \text{g}^{-1}$ and the best electrical conductivity.

Electromechanical properties

Figure 7a was the displacement curves of actuators with different mass fractions of MCNT and RGO at $5\text{ V } 0.05\text{ Hz}$. Here, we carried out five experiments on the sample under the same experimental condition, and the average peak value of displacement was obtained. It can be seen from the observation that the deflection displacement of the actuators at different doping ratios showed a periodic variation trend. By comparison, actuators with electrode layer of 0.11% RGO and 0% MCNT exhibited no significant periodic deflection displacement under $5\text{ V } 0.05\text{ Hz}$. Actuators with electrode layer of 0.1% RGO and 1.3% MCNT had the maximum cyclic deflection displacement. The maximum peak to peak displacement peak was 2.67 mm , which as 2.19 times than the minimum value. The experimental results of actuation

performance were basically consistent with the results of electrochemical analysis results. Figure 7b showed the peak to peak deflection displacement of actuators at $5\text{ V } 0.05\text{--}2\text{ Hz}$. From the observation, it can be seen that as the frequency increased, the peak value of the deflection displacement showed a decreasing trend. The analysis results showed that there was no significant periodic deflection displacement of actuators with the electrode layer with 0.11% RGO and 0% MCNT at $5\text{ V } 0.05\text{--}2\text{ Hz}$. Actuators with electrode layer of 0.11% RGO and 1.3% MCNT had a maximum peak value of 0.849 mm , which was 3.64 times than the minimum value at $5\text{ V } 0.1\text{ Hz}$. The electromechanical properties of actuators had been significantly improved. This illustrated the rationality of the internal structure of electrode layer to improve the electromechanical performance of actuators.

Above all, carbon atoms in MCNT were mainly composed of sp^2 hybrids and form a curved hexagonal grid structure, which was a spatial topology. And RGO was two-dimensional carbon nanomaterial composed of carbon atoms in the form of sp^2 hybrid orbitals, which consisted of a hexagonal honeycomb structure. Chitosan dissolved in acetic acid, and formed a stable lattice structure. After doping with cellulose, the electrode layer formed a large number of porous structures, which was served as a good skeleton. When the electrode membrane solution was stirred and mixed with conductive particles, a large number of MCNT adhered to RGO to form a clad block structure, which greatly increased the specific surface area of the conductive particles of the electrode layer, and effectively utilized the pores structure generated in

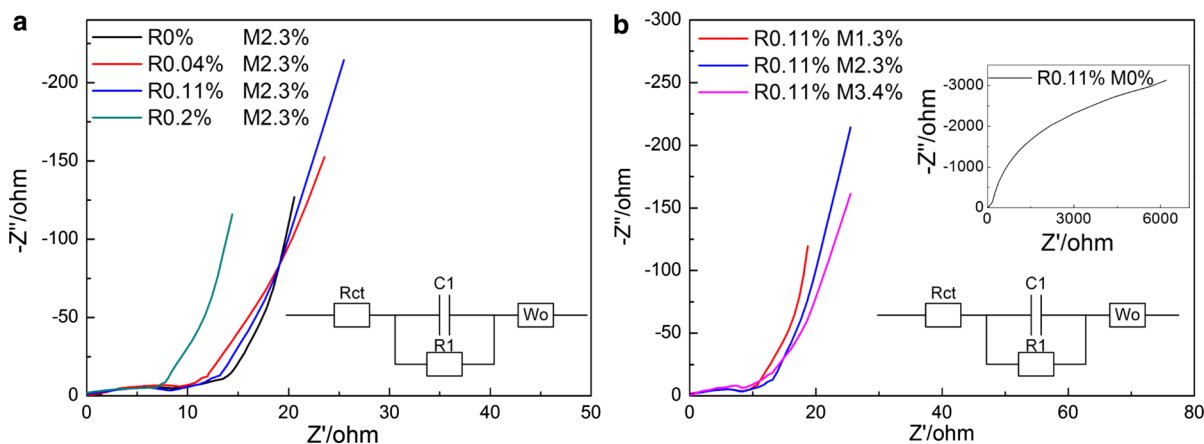


Fig. 6 EIS curves of electrode layers with different mass fractions MCNT and RGO at $10^{-5}\text{--}0.01\text{ Hz}$

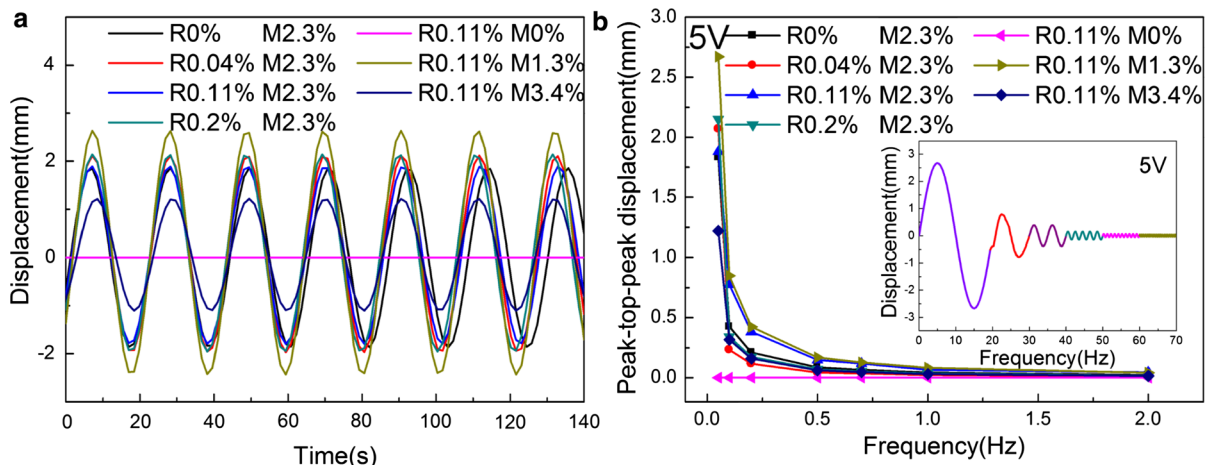


Fig. 7 Deflection peak to peak displacement curves of actuators: **a** different mass fractions at 5V 0.05 Hz **b** different frequency at 5 V 0.05–2 Hz

chitosan and cellulose skeleton. After voltage excitation of actuators, the porous structure not only provided a large number of channels for electrons to flow through, but also MCNT and RGO in the porous structure greatly enhanced the conductivity of the electrode layer, which resulted in the improvement of electrochemical and electromechanical properties of actuators.

Conclusion

In summary, in this paper, we developed a high performance Re-Cel nanocomposite soft actuator based on porous high-conductivity electrode membrane, which was composed of porous framework formed by biopolymer cellulose-mixed chitosan and highly conductive nanoparticle generated by reduced RGO–MCNT. Results demonstrated that actuators based on prepared electrode layer without regenerated substance according to the tested results from FT-IR and XRD exhibited significant enhancement in the peak to peak displacement, which was 3.64 times increased than the minimum value at 5 V 0.1 Hz with electrode layer of 0.11% RGO and 1.3% MCNT. Also, it showed a maximum peak displacement of 2.67 mm at 5 V 0.05 Hz, which as 2.19 times than the minimum value.

The main reasons for experimental results of the absolute advantages of prepared electrode layer in the conductivity and channels for electrons were that chitosan doped with cellulose formed a large number

of porous structures, which were served as a polymer skeleton. A large number of MCNT adhered to RGO to generate a clad block structure, which greatly increased the specific surface area of the conductive particles of the electrode layer, and effectively utilized the pores structure generated in chitosan and cellulose skeleton. After voltage excitation of actuators, the porous structure provided a large number of channels for electrons to flow through, and MCNT and RGO in the porous structure greatly enhanced the conductivity of the electrode layer, which resulted in the enhancement of electrochemical and electromechanical properties of actuators.

Acknowledgments We gratefully acknowledge the financial support by China Postdoctoral Science Foundation Funded Project (Grant No. 2018M630330), Natural Science Foundation of Heilongjiang Province (Grant No. QC2018046), National Science Foundation of China (Grant No. 31470714), and Fundamental Research Funds for the Central Universities (Grant No. 2572017BB08).

References

- Acerce M, Akdoğan EK, Chhowalla M (2017a) Metallic molybdenum disulfide nanosheet-based electrochemical actuators. *Nature* 549(7672):370
- Acerce M, Akdoğan EK, Chhowalla M (2017b) Metallic molybdenum disulfide nanosheet-based electrochemical actuators. *Nature* 549(7672):370
- Acome E, Mitchell SK, Morrissey TG (2018) Hydraulically amplified self-healing electrostatic actuators with muscle-like performance. *Science* 359(6371):61–65

- Altinkaya E, Seki Y, Yılmaz ÖC (2016) Electromechanical performance of chitosan-based composite electroactive actuators. *Compos Sci Technol* 129:108–115
- Barrios CA (2018) A deflection optical sensor based on a Scotch tape waveguide with an integrated grating coupler. *Sens Actuators A Phys* 269:500–504
- Chen J, Huang X, Zhu Y (2017) Cellulose nanofiber supported 3D interconnected BN nanosheets for epoxy nanocomposites with ultrahigh thermal management capability. *Adv Funct Mater* 27(5):1604754
- Fang X, Li A, Yildiz O (2017) Enhanced anisotropic response of dielectric elastomer actuators with microcombed and etched carbon nanotube sheet electrodes. *Carbon* 120:366–373
- Jang KI, Li K, Chung HU (2017) Self-assembled three dimensional network designs for soft electronics. *Nat Commun* 8:15894
- Kim SS, Jeon JH, Kim HI (2015) High-fidelity bioelectronic muscular actuator based on graphene-mediated and tempoxidized bacterial cellulose. *Adv Funct Mater* 25(23):3560–3570
- Kotal M, Kim J, Kim KJ (2016a) Sulfur and nitrogen co-doped graphene electrodes for high-performance ionic artificial muscles. *Adv Mater* 28(8):1610–1615
- Kotal M, Kim J, Kim KJ (2016b) Sulfur and nitrogen co-doped graphene electrodes for high-performance ionic artificial muscles. *Adv Mater* 28(8):1610–1615
- Lasprilla AJR, Martinez GAR, Lunelli BH (2012) Poly-lactic acid synthesis for application in biomedical devices-A review. *Biotechnol Adv* 30(1):321–328
- Lu L, Liu J, Hu Y (2012a) Highly stable air working bimorph actuator based on a graphene nanosheet/carbon nanotube hybrid electrode. *Adv Mater* 24(31):4317–4321
- Lu L, Liu J, Hu Y (2012b) Large volume variation of an anisotropic graphene nanosheet electrochemical-mechanical actuator under low voltage stimulation. *Chem Commun* 48(33):3978–3980
- Lu L, Liu J, Hu Y (2013) Graphene-stabilized silver nanoparticle electrochemical electrode for actuator design. *Adv Mater* 25(9):1270–1274
- Muralidharan MN, Shinu KP, Seema A (2016) Optically triggered actuation in chitosan/reduced graphene oxide nanocomposites. *Carbohydr Polym* 144:115–121
- Ozdemir O, Karakuzu R, Sarikanat M (2015) Effects of PEG loading on electromechanical behavior of cellulose-based electroactive composite. *Cellulose* 22(3):1873–1881
- Sun Z, Zhao G, Song W (2017a) A naturally crosslinked chitosan based ionic actuator with cathode deflection phenomenon. *Cellulose* 24(2):441–445
- Sun Z, Song W, Zhao G (2017b) Chitosan-based polymer gel paper actuators coated with multi-wall carbon nanotubes and MnO₂ composite electrode. *Cellulose* 24(10):4383–4392
- Terasawa N, Asaka K (2017) High-performance polymer actuators based on an iridium oxide and vapor-grown carbon nanofibers combining electrostatic double-layer and faradaic capacitor mechanisms. *Sens Actuators B Chem* 240:536–542
- Terasawa N, Asaka K (2018) High-performance graphene oxide/vapor-grown carbon fiber composite polymer actuator. *Sens Actuators B Chem* 255:2829–2837
- Wang F, Jeon JH, Park S (2016) A soft biomolecule actuator based on a highly functionalized bacterial cellulose nanofiber network with carboxylic acid groups. *Soft Matter* 12(1):246–254
- Wang D, Lu C, Zhao J (2017a) High energy conversion efficiency conducting polymer actuators based on PEDOT:PSS/MWCNTs composite electrode. *RSC Adv* 7(50):31264–31271
- Wang Y, Qian J, Zhao N (2017b) Novel hydroxyethyl chitosan/cellulose scaffolds with bubble-like porous structure for bone tissue engineering. *Carbohydr Polym* 167:44–51
- Wu G, Hu Y, Liu Y (2015) Graphitic carbon nitride nanosheet electrode-based high-performance ionic actuator. *Nat Commun* 6:7258
- Xin Y, Xiong Q, Bai Q (2017) A hierarchically porous cellulose monolith: a template-free fabricated, morphology-tunable, and easily functionalizable platform. *Carbohydr Polym* 157:429–437
- Yuk H, Lin S, Ma C (2017) Hydraulic hydrogel actuators and robots optically and sonically camouflaged in water. *Nat Commun* 8:14230